Volume 16, Number 4, 2023. pp. 381-393

Jordan Journal of Physics

ARTICLE

Monte Carlo Simulation of Free-standing Thin Films under Low Energy Electron Bombardment: Electron Inelastic Mean Free Path (IMFP) Determination Using Elastic Peak of the Transmitted Electrons

Ahmad M.D. (Assa'd) Jaber[a], **H. H. Kawariq**[b], **C. G. H. Walker**[c,d] and **Marwan S. Mousa**[e]

[a] *Department of Basic Medical Sciences, Faculty of Medicine, Aqaba Medical Sciences University, Aqaba, 77110, Jordan.*

[b] *Department of Mathematics, Faculty of Science, Philadelphia University, Jerash, Jordan.*

[c] *Laboratorium für Festkörperphysik, Auguste-Piccard-Hof 1, 8093 Zürich, Switzerland.*

[d] *Department of Physics, University of York, Heslington, York, YO10 5DD, UK.*

[e] *Department of Physics, Mu'tah University, P.O.Box (7), Al-Karak, Jordan.*

Doi: https://doi.org/10.47011/16.4.1

Received on: 23/08/2022; *Accepted on: 25/10/2022*

Abstract: The electron energy spectra of transmitted scattered electrons from free-standing films are simulated using a Monte Carlo computational approach. Elastic scattering is simulated using Mott cross-sections and inelastic scattering via discrete processes determined from dielectric function data. This allows one to simulate the secondary electrons as well as the loss peaks near the elastic (zero-loss) peak. The current study suggested a directed approach for determining the electron inelastic mean free path (IMFP) of materials at low primary electron energies. The IMFP of the reference material is not necessary for the suggested technique. The suggested technique uses the ratio between the transmitted elastic peak intensity and the background intensity of backscattered electrons. Free-standing films of Si, Cu, and Au were studied with thicknesses varying from 2 to 12 nm. Primary electron energies of 1, 3, and 5 keV were applied. The results appeared very good, with the percentage error range being between 5% and 25%. We also investigated the proportion of the first and second plasmon peak intensities to the elastic peak intensity. We believe that the latter could provide a directed method of measuring the IMFP of materials.

Keywords: Inelastic mean free path, Monte Carlo simulation, Geant4, Free-standing film, Zero-loss peak.

1. Introduction

Low Voltage Scanning Electron Microscopy (LVSEM) has been growing in popularity in recent years due to its improved spatial resolution [1]. However, the Auger and Energy-dispersive X-ray spectroscopy (EDX) signals are less intense as a result of the lower beam energy. This makes characterizing the sample more challenging. It is well known that the shape of the background in electron energy spectra varies according to the atomic number, making it a valuable tool for material characterization. The commonly used Backscattered Electron Detector (BSD) can be employed to determine changes in the substrate atomic number. However, BSDs are mostly based on p-n junctions and have a detection threshold of 1-2 keV, rendering them

Corresponding Author: Ahmad M.D. (Assa'd) Jaber **Email**: ahmad.jabr@amsu.edu.jo

less effective when dealing with a primary energy of 1 keV. Therefore, more detailed information could be obtained from a broad energy spectrum. For instance, determining that a sample is an alloy of a high and a low atomic number material rather than a single element in the middle of the periodic table [2-4].

Many methods for the characterization of graphene [5] and other 2D materials [6] have emerged since their introduction [7]. The preferred method for studying 2D materials is employing electron beam technologies because the sample size can often be very small. The combination of electron spectroscopic techniques with both transmission and reflection electron microscopy opens up powerful approaches to studying these materials. Konvalina *et al.* [8] recently acquired electron spectra from a 50 eV primary electron beam transmitted through graphene. The spectra were acquired using a novel time-of-flight technique. Scanning Low Energy Electron Microscopy (SLEEM) was used to lower the energy of the electrons before they were transmitted through the material [9]. Transmission spectra using low energy electrons have been obtained from polymer films [10], molecular solids [11], and biomolecular solids [12].

Walker *et al.* [13] have studied electron transmission through free-standing Si and Au films (100 nm thickness) with 15 and 30 keV beams using Scanning Electron Microscopy (SEM) in Scanning Transmission Electron Microscopy (STEM) mode. The degree of angular scattering was compared with Monte Carlo simulations. According to Konvalina *et al*. [8], the study of electron spectra after transmission through thin films can be used to determine quantitative information regarding electron transport. Werner [14] has used a Reflection Electron Energy Loss (REELS) technique for determining dielectric functions, and a similar approach could be used in transmission Electron Energy Loss Spectroscopy (EELS). Cazaux [15] considered the transmission of electrons through thin free-standing films. However, he was concerned with very low energy. Interestingly, he found that the transmission probability oscillated according to the energy of the electron. Oscillations in the probability of electron transmission through graphene were also predicted using DFT calculations [16].

The use of EELS in determining the thickness of samples is widely used in Transmission Electron Microscopy (TEM) [17-19]. However, the used method requires low levels of multiple scattering and the presence of secondary electrons suggests that the usual approach used in TEM might not work so well at such low primary beam voltages. The study of thin films on surfaces and the determination of the thickness via the overlayer technique has been widely used in Auger Electron Spectroscopy (AES) and X-ray Photoelectron Spectroscopy (XPS) [20]. In earlier research, it was assumed that the signal decayed exponentially, however, this neglected the impact of elastic scattering [21]. In addition, the overlayer technique measures the exponential decay of a peak (Auger or photoelectron) and this provides a measure of the effective attenuation length (EAL) (i.e. the distance traveled for a loss of 1/e in the signal), which is not the same as the inelastic mean free path (IMFP) (which is defined as the mean distance between inelastic events) [21]. In TEM, no distinction is made between EAL and IMFP due to the high beam energies used. As the beam energy is reduced, this distinction should be taken into consideration. However, for simplicity, we will regard the EAL and IMFP as equivalent and will discuss how to treat the EAL and IMFP in transmission in a future report.

Thus, in XPS, AES, and EELS, sample thickness and quantitative surface characterisation depend on an understanding of the electron inelastic mean free path (IMFP) and its energy dependency. Theoretical values of the inelastic mean free path (IMFP) and their electron-energy dependence are available in the literature from predictive formulae for various categories of materials. In a series of studies, Tanuma *et al.* and Shinotsuka *et al*. [22-24] estimated the inelastic mean free path values for various materials, including a group of 41 elemental solids, 15 inorganic compounds, and 14 organic compounds. The results of these studies revealed a general formula for calculating the inelastic mean free path value, which is known as the TPP-2M. In their experimental measurements, Tanuma *et al.* and Shinotsuka *et al*. employed Elastic Peak Electron Spectroscopy (EPES) to measure the inelastic mean free path (IMFP) for both the reference materials and the targeted materials. The reference elements were used to avoid

measurement of the elastic reflection coefficient in absolute units [22-24].

In this study, we are interested in primary electron energies of 1, 3, and 5 keV. These energy levels encompass the range of beam voltages employed in low voltage scanning electron microscopy in the transmission mode [25, 26]. We used Monte Carlo (MC) methods to investigate how the transmitted electron spectra change with film thickness for three different materials with significantly varying atomic numbers: Si, Cu, and Au. The aim of this study is to propose a novel method for calculating the Si, Cu, and Au electron inelastic mean free paths (IMFPs) at different primary electron energies. The method uses the ratio of transmitted elastic peak intensity to the backscattered electron background intensity. In the suggested approach, the value of the IMFP of the reference material is not required for calculating the IMFP of the targeted materials. Moreover, the novelty of the method suggested here is that discrepancies between the sample being studied and the reference materials are eliminated.

2. Monte Carlo Simulations

The MC program used in this study was developed by Kieft and Bosch [27] and uses the Geant4 set of libraries [28]. The program uses Mott cross-sections to calculate the elastic scattering [29]. The program also uses inelastic scattering discrete inelastic losses, with each energy loss used to generate a secondary electron (SE) with the same energy as that lost by the initial electron (usually a primary electron (PE) but could also be another SE). The inelastic losses were determined from dielectric function data, as described by Werner [30]. As such, the MC model does not include losses due to surface plasmons. All electrons escaping from the film were used to generate the electron spectra, i.e., no angularly resolved data was acquired.

The present work conducted a study on free-standing Si, Cu, and Au thin films of varying thicknesses. With normal incidence, the energy of the primary beam was set to 1, 3, and 5 keV. Transmitted spectra consisting of forward-scattered electrons have been collected. In Fig. 1, the energy loss function (ELF) is shown for Si, Cu, and Au with log scales on both axes. The ELF shows the energy distribution of the SEs at their point of generation. Take note of the strong bulk plasmon peak in Si (at ~16 eV), which leads to intense plasmon loss peaks. In contrast, the Au and Cu bulk plasmon loss peaks are more complex (between ~5 and ~50 eV), which will lead to a complex plasmon loss structure.

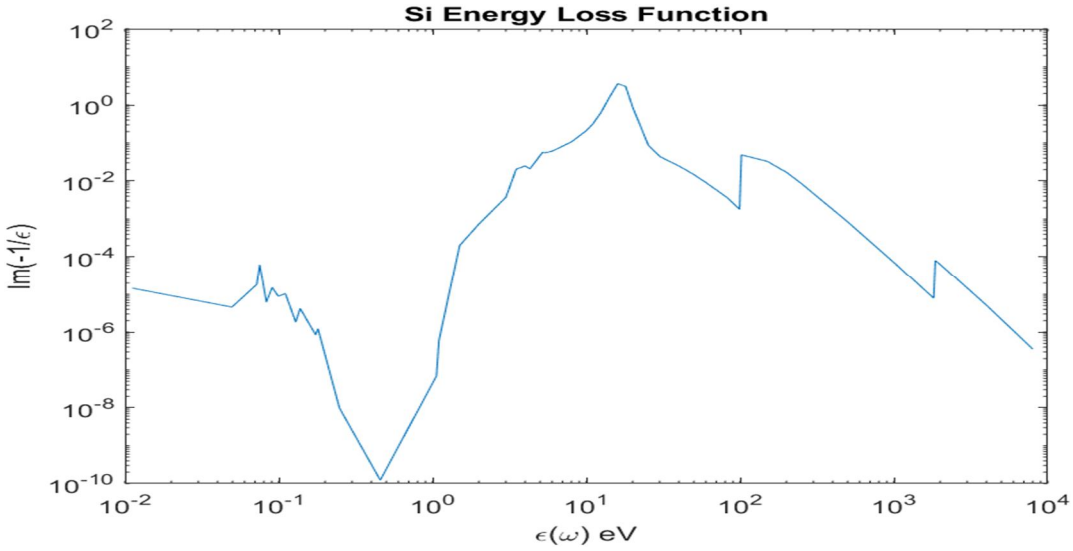

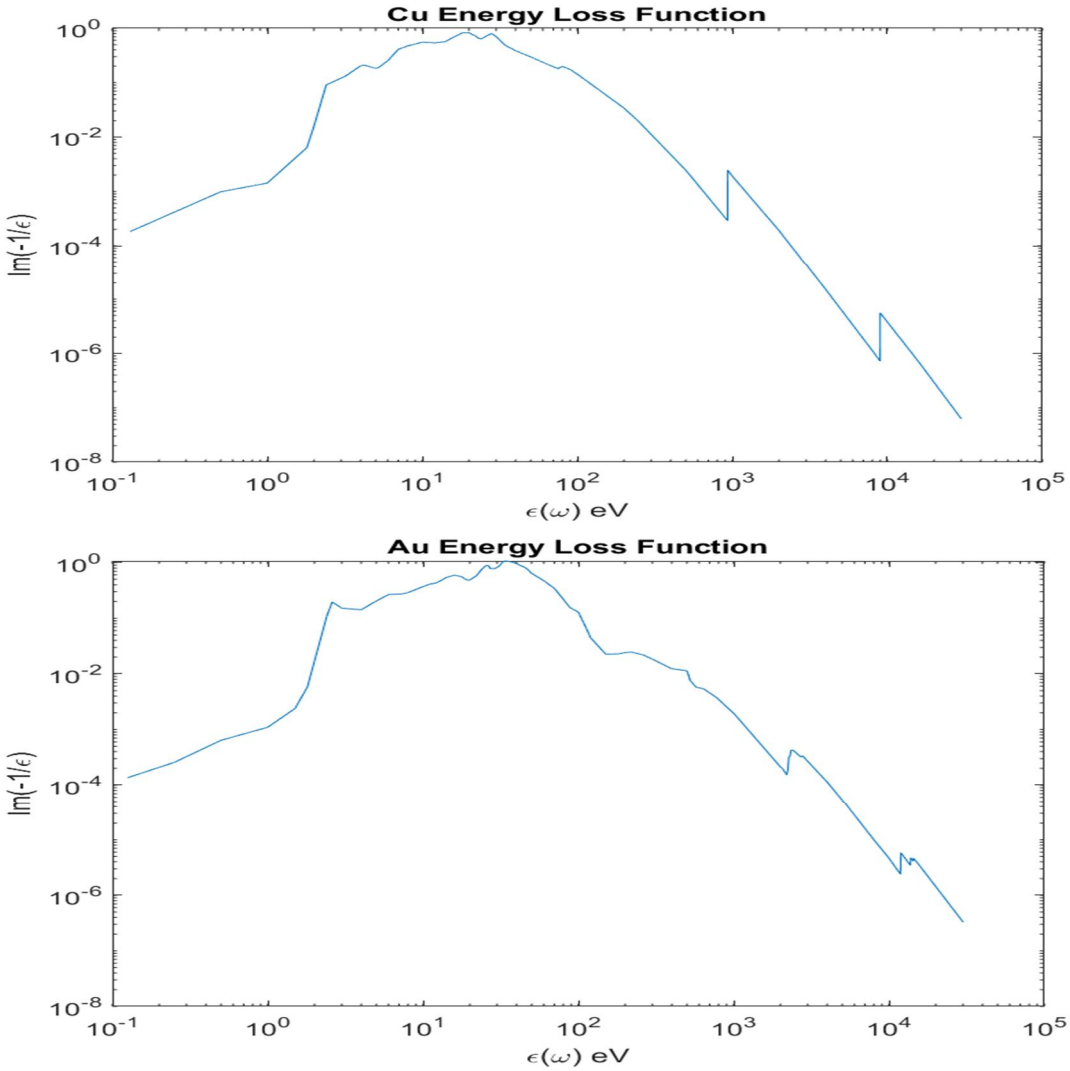

FIG. 1. Electron energy loss function (ELF) derived from dielectric function data for Si, Cu, and Au. Log scale on both axes. Data as used by Kieft and Bosch [27] who obtained their data from Palik [31].

3. Results

Figures 2, 3, and 4 show the simulated electron energy spectrum of transmitted electrons for Si, Cu, and Au films, respectively, of various thicknesses at different primary beam energies of 1, 3, and 5 keV. Strong changes occur, especially in the region of the secondary electron (i.e. E_p < 50 eV), the figure in the box on the left side, and plasmon loss peaks in the figure on the right side. Generally, the secondary electron yield increases as the layer thickness increases. This is due to the fact that, as the layer thickness increases, the primary electrons travel a greater distance within the layer and more inelastic scattering events take place, producing more secondary electrons. In the case of 1 keV primary electron energy for Cu and Au, the secondary electron yield increases as the layer thickness increases until it reaches its maximum intensity at 6 nm for Cu and 4 nm for Au, and then starts decreasing for layer thicknesses larger than 6 and 4 nm for Cu and Au, respectively. This is due to the main part of the electron solid interaction volume becoming at a distance from the transmitted surface larger than the secondary electron path length.

The intensity of the elastic peak (no energy loss peak) of the transmitted electron spectrum decreases as the layer thickness increases. On the other hand, BSE electrons (50 eV < BSE < E_p) in the background of the spectrum increase as the layer thickness increases. As the layer thickness increases, the primary electrons will suffer more inelastic and elastic scattering events. So, the primary electrons will suffer energy loss before transmitting. However, the plasmon peaks show different behavior in the collected transmitted electron spectra. Generally, in the case of 1 keV, the plasmon peaks are decreasing as the film thickness increases. At 3 and 5 keV for Si film,

the first plasmon peak starts increasing as the film thickness increases until it reaches its maximum intensity and starts decreasing for thicknesses greater than 4 and 8 nm for 3 and 5 keV, respectively. In the case of Cu and Au films at 3 and 5 keV, the plasmon peaks increase as the layer thickness increases until reaching 4 nm, at which thickness they start to decrease. This phenomenon can also be attributed to the effective primary electron energy, which has the capability of generating plasmon electrons through inelastic collision.

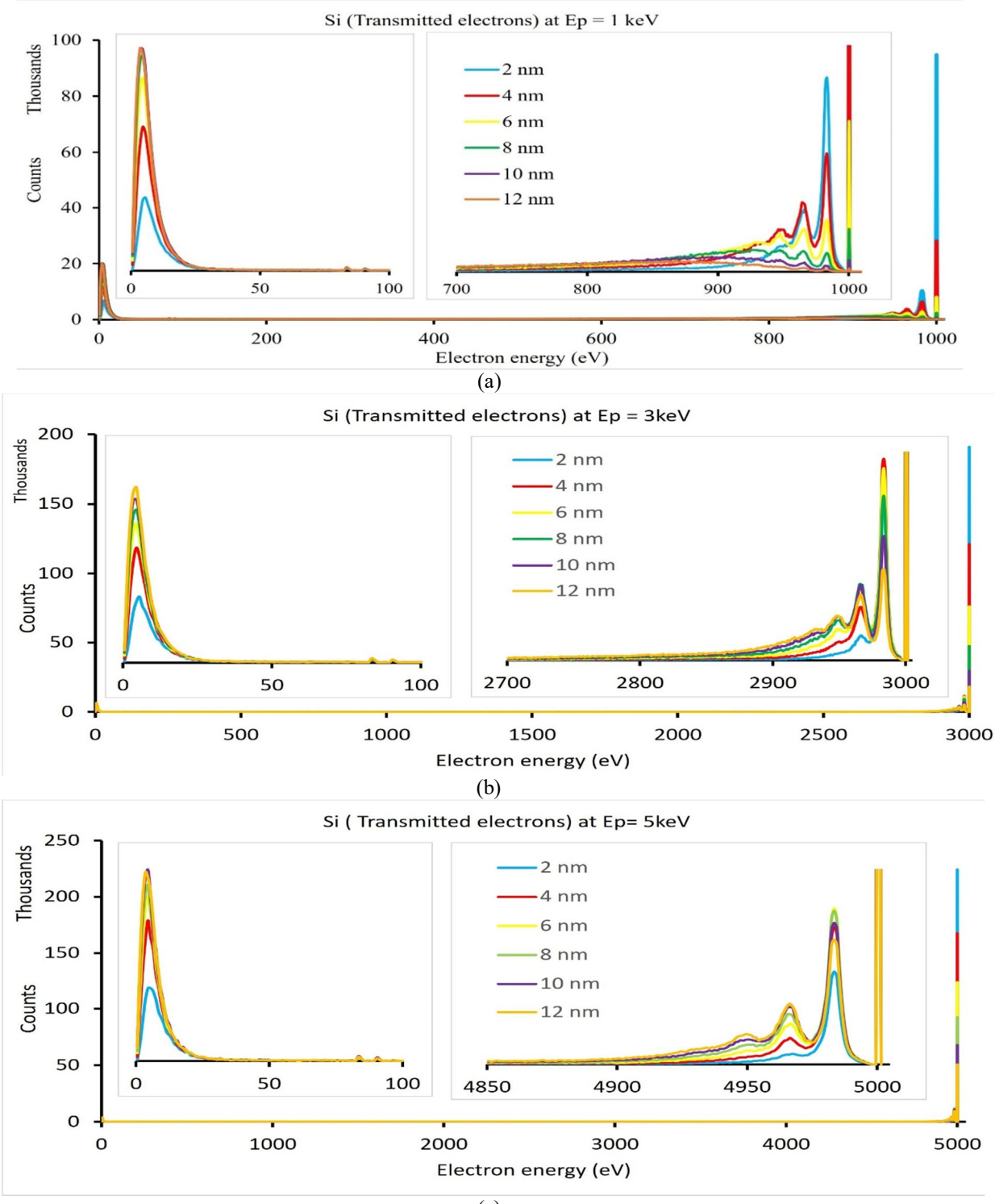

FIG. 2. Energy distribution of the transmitted electrons of Si for free-standing films with thicknesses from 2 to 12 nm for a primary beam energy of E_p = 1 keV (a), 3 keV (b), and 5 keV (c). The number of primary beam electrons for each spectrum is 300 k.

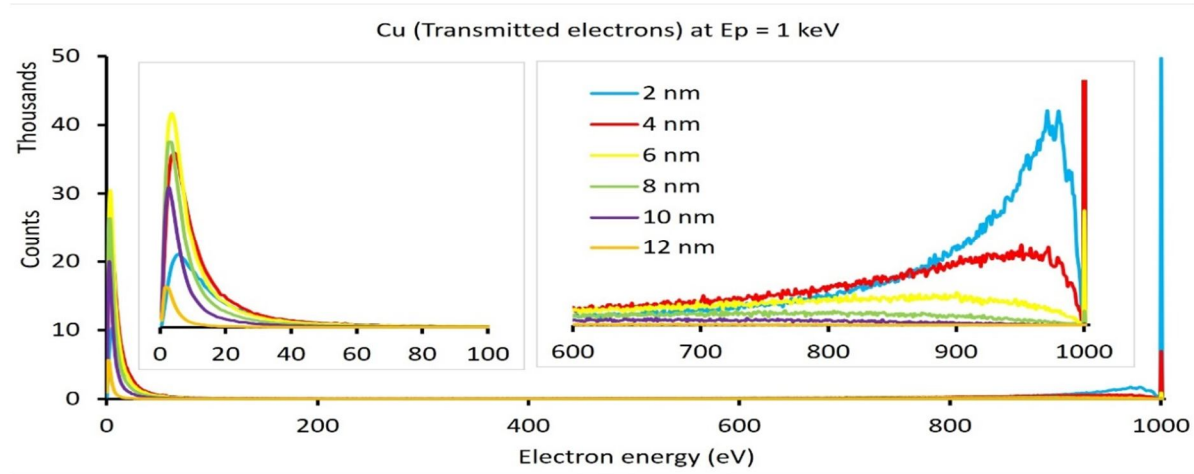

(a)

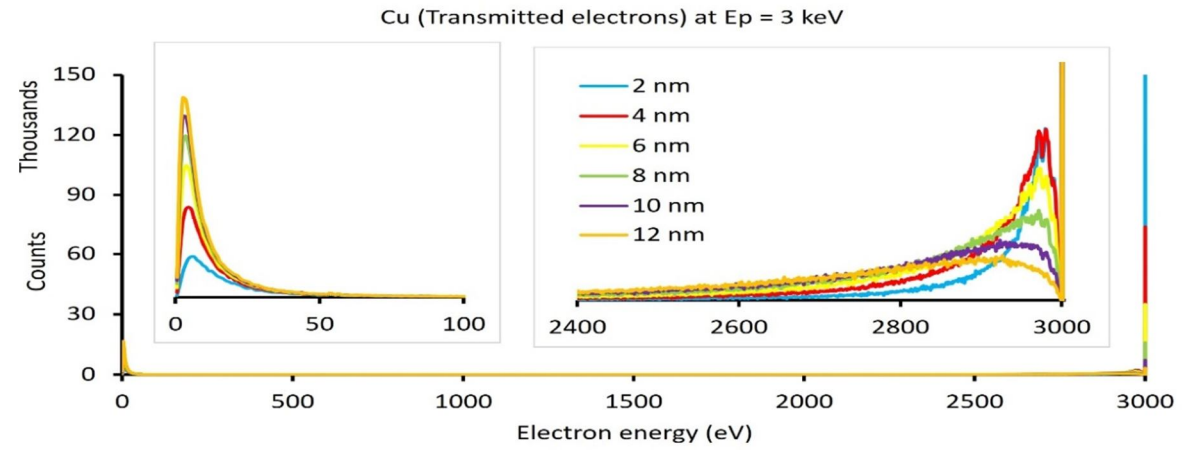

(b)

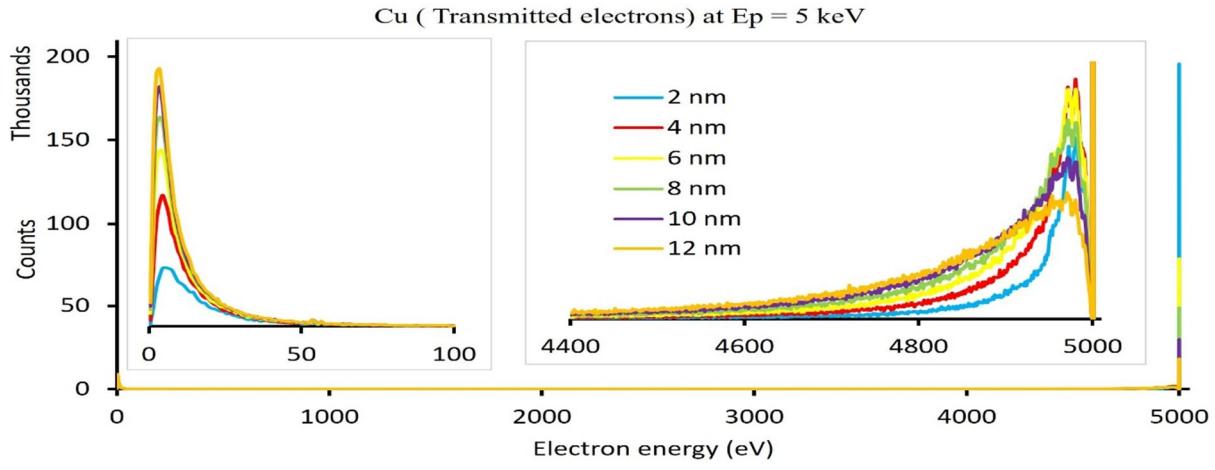

(c)

FIG. 3. Energy distribution of the transmitted electrons of Cu for free-standing films with thicknesses from 2 to 12 nm for a primary beam energy of E_p = 1 keV (a), 3 keV (b), and 5 keV (c). The number of primary beam electrons for each spectrum is 300 k.

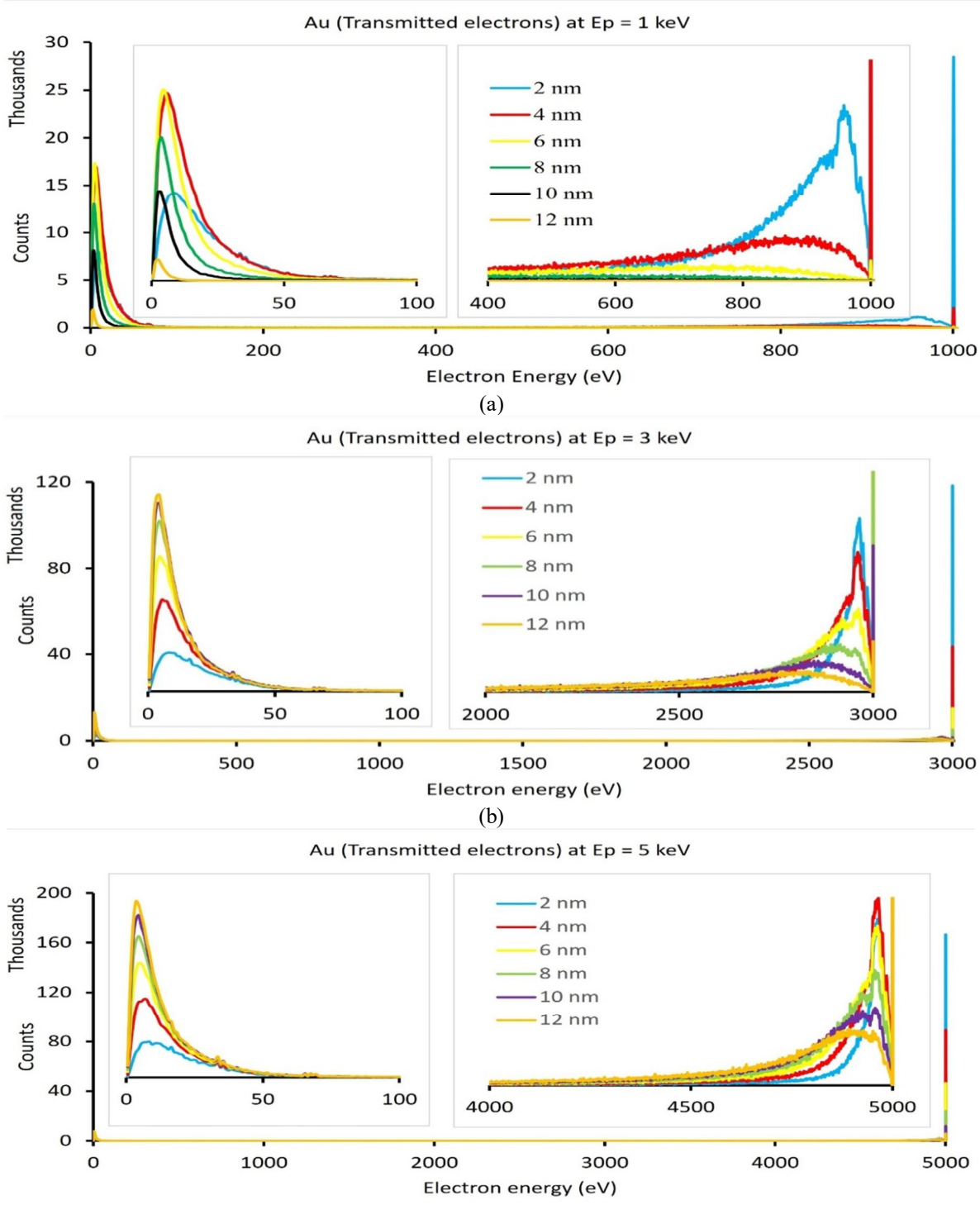

FIG. 4. Energy distribution of the transmitted electrons of Au for free-standing films with thicknesses from 2 to 12 nm for a primary beam energy of E_p = 1 keV (a), 3 keV (b), and 5 keV (c). The number of primary beam electrons for each spectrum is 300 k.

4. Discussion

In the case of Si, the transmitted electron spectra show a small background intensity for thin films as compared to the bulk. This is clearer at around half the primary beam energy and above. The background at half the primary beam energy is low at a small film thickness since there are few electron energy losses within the film, causing few electrons to be transmitted and collected at these electron energies. As the film thickness increases, the intensity at this mid-range climbs to a maximum at about 10 nm

and then falls again. This behavior is due to the primary electrons having lost about half their energy by about 12 nm depth. The intensity of the spectrum begins to decrease at higher energy levels as the film thickness increases. This should be expected, as the electrons lose energy from the primary beam and thus cause an increase in the number of electrons with lower energies for thicker films.

In the case of Cu and Au, similar behavior is seen to that of Si, but for much thinner films. The spectrum rises in intensity at a mid-range between 2 and 4 nm, but for thicker samples the count rate drops. For the 10 nm thick film, the spectrum is almost flat between 200 and 600 eV and at an intensity ~10 times lower than the 2 or 4 nm thick films. For the 12 nm thick film, only the low-energy SEs are emerging from the surface. One point of interest in this study is that the background is almost flat in the mid-range energies for the thicker films. Auger peaks in this energy range would only have a weak intensity due to the low primary beam energy. Hence, an energy spectrometer with a very coarse bandwidth acquiring data over a wide energy range could perhaps be used as a film thickness monitor in some industrial processes where many almost identical samples are expected.

The multiple plasmon loss peaks shown here can also be seen in EELS spectra acquired with a Transmission Electron Microscope (TEM). The intensity of a given plasmon loss peak can be described by Poisson statistics [17]:

$$P_n = \frac{1}{n!}\left(\frac{t}{\lambda}\right)^n exp(-t/\lambda) \quad (1)$$

where P_n is the probability of exciting the n^{th} plasmon, t is the specimen thickness, and λ is the mean free path (MFP) for plasmon scattering.

For n = 0, the intensity of the zero-loss peak is given by [17]:

$$P_0 = \exp\left(-\frac{t}{\lambda}\right) = \frac{I_0}{I_t} \quad (2)$$

where I_0 is the integral intensity under the zero-loss (elastic) peak and I_t is the integral under the whole spectrum (including the zero-loss peak). Using Eq. (2), an estimate of the sample thickness can be made [19] if we know λ of the specimen. This technique works well at the high incident beam energies that are experienced in TEM. Equation (2) simply expresses the exponential decay of the beam due to inelastic scattering and therefore one might expect it to be also valid at lower primary beam energies (e.g. down to 5 keV). However, it is uncertain whether the approach at such energies is due to the effects of elastic scattering and the contribution of secondary electrons to I_t. It is unclear how to set the lower energy limit for determining I_t. In our case, we chose the conventional energy limit of the backscattered electrons, which was 50 eV, as the lower energy limit. One can see the contribution from secondary electrons starts to increase below this value (see Figs 2, 3, and 4).

Figures 5, 6, and 7 were obtained from running the MC model for the natural log ratio of I_0/I_t versus film thickness and fitting straight lines for Si, Cu, and Au films, respectively, at E_P of 1, 3, and 5 keV. From the slope of the fitted lines, one can determine the inelastic mean free path length (λ) of the electron in Si, Cu, and Au materials. Table 1 shows the λ values obtained from the input data of the Geant-4 MC model [27], present Monte Carlo simulation (MC), plus using Eq. (2) and the IMFP data from Ref. [22] for comparison with some results in the literature. The results of the MC simulation (fitted line in Fig. 5) are nearly identical to the results of the Geant-4 program [27]. The difference between the two data sets is between 4% and 20%. The results of the present MC simulation are considerably lower than those in the literature. The influence of elastic scattering causes the path length traversed to be lower than a straight-line path [21]. This effect needs to be accounted for if one is to determine the correct film thickness using low-energy TEM experiments. Also, the calculations above assume the acquisition of all transmitted electrons, which may not be the case when using an electron energy analyzer with a small entrance aperture. The calibration with films of known thickness should help to overcome this problem and would obviate the need to know the value of the MFP (λ) in advance. In addition, unlike in the TEM, the EELS spectrum is normally acquired sequentially, which will be quite time-consuming. Care must be taken with very thin films not to overwhelm any detector (e.g., channeltron) tuned to the zero-loss peak. Possibly, one could use a high pass energy filter tuned to acquire the zero-loss peak and then tuned to acquire all electrons above the low energy limit. Such a filter would be relatively simple to construct.

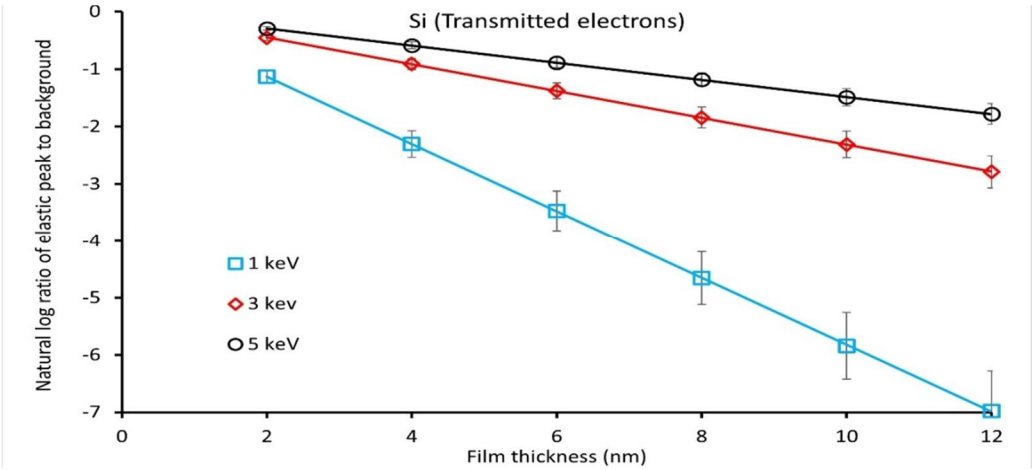

FIG. 5. Natural log of the ratio of the area under the background (from 50 eV to above the elastic peak) to the area under the zero-loss peak for Si. The fitted curves are shown in red. For 1 keV, the fitted curve is given by $y = -(0.586 \pm 0.002)\,x + (0.037 \pm 0.012)$, for 3 keV $y = -(0.233 \pm 0.001)\,x + (0.015 \pm 0.006)$, and for 5 keV $y = -(0.149 \pm 0.001)\,x + (0.004 \pm 0.004)$.

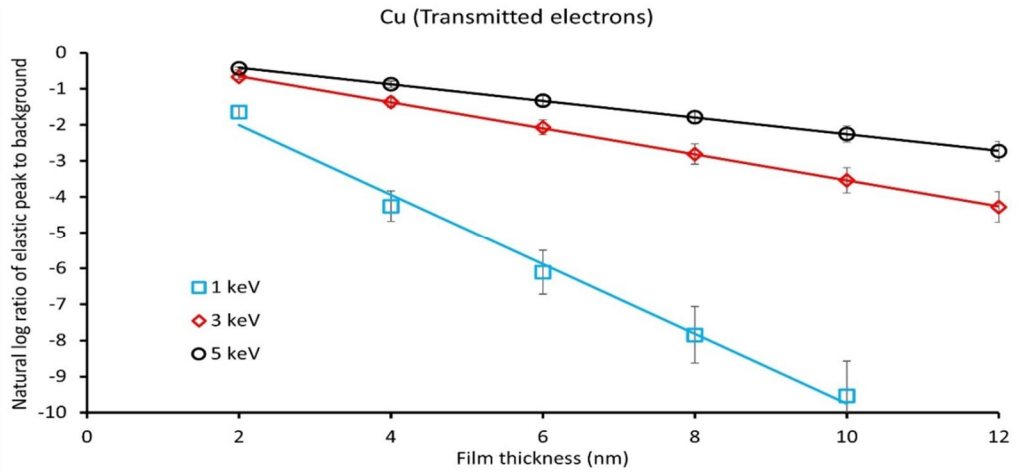

FIG. 6. Natural log of the ratio of the area under the background (from 50 eV to above the elastic peak) to the area under the zero-loss peak for Cu. The fitted curves are shown in red. For 1 keV, the fitted curve is given by $y = -(0.968 \pm 0.053)\,x - (0.069 \pm 0.348)$, for 3 keV $y = -(0.361 \pm 0.002)\,x + (0.072 \pm 0.017)$, and for 5 keV $y = -(0.229 \pm 0.002)\,x + (0.041 \pm 0.013)$.

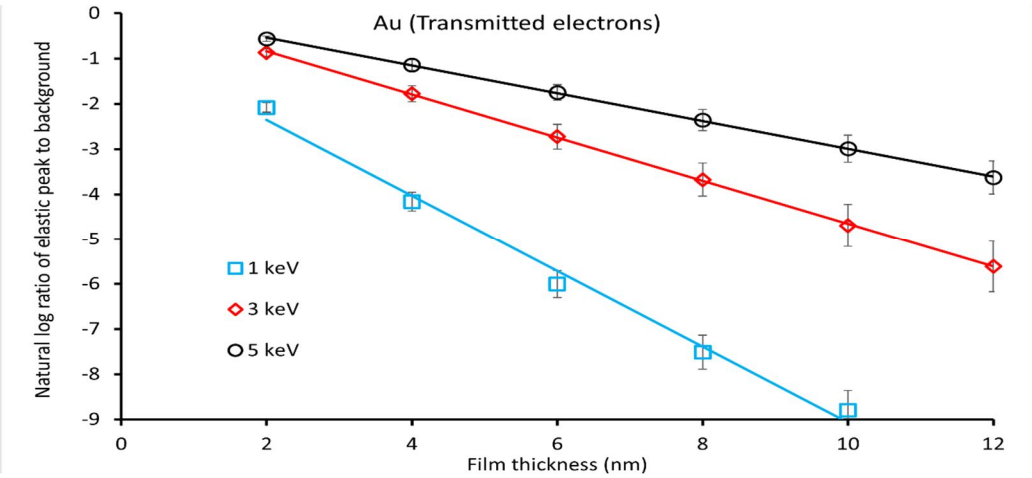

FIG. 7. Natural log of the ratio of the area under the background (from 50 eV to above the elastic peak) to the area under the zero-loss peak for Au. The fitted curves are shown in red. For 1 keV, the fitted curve is given by $y = -(0.839 \pm 0.05)\,x - (0.677 \pm 0.31)$, for 3 keV $y = (-0.477 \pm 0.004)\,x + (0.117 \pm 0.028)$, and for 5 keV $y = -(0.307 \pm 0.003)\,x + (0.075 \pm 0.022)$.

TABLE 1. IMFP (in nm) as a function of electron energy for Si, Cu, and Au.

	Si			Cu			Au		
E_p	Input data Ref. [27,28]	MC	Data Ref. [22]	Input data Ref. [27,28]	MC	Data Ref. [22]	Input data Ref. [27,28]	MC	Data Ref. [22]
1 keV	1.9	1.7	2.39	1.4	1.03	1.5	1.13	1.2	1.23
3 keV	4.5	4.3	5.79	3.3	2.8	3.6	1.7	2.1	2.8
5 keV	6.9	6.7	8.87	4.9	4.4	5.5	3.93	3.3	4.3

Another option would be to plot the intensity of the individual plasmon loss peaks as a function of film thickness. Equation (1) suggests that the intensity of the first plasmon loss peak compared with the zero-loss peak should be linear. On the other hand, for the second loss peak, the relationship should be quadratic. These peaks could be acquired relatively rapidly with a short energy range scan near the zero-loss peak. Therefore, in Fig. 8, we have plotted this data in the case of Si. It would be expected that Eqs. (1) and (2) would only be valid at small film thicknesses due to multiple scattering and geometric effects. The linear nature of the ratio of the first plasmon peak to the zero-loss peak ratio is evident. The quadratic nature of the second peak is not so obvious, but if one makes the valid assumption that the curve should pass through zero and ignores the point at 12 nm (due to multiple scattering effects), then a reasonable fit occurs. The slope for the fit to the first plasmon peak suggests a characteristic length due to plasmon losses of about 4.5 nm, which is ~50% longer than that depicted in Fig. 5. However, the path length determination depends on how many loss events one includes. The fewer losses, the longer the path length one can expect to derive. The point is that one can also use this approach after calibration to determine film thickness. Since the peak is close to the elastic peak, data would be quicker to acquire, given that a majority of electron energy analysers obtain spectra serially. Alternatively, with a simple high-pass filter, one might be able to acquire the I_t and I_o signals using Eq. (2) and rapidly determine film thickness.

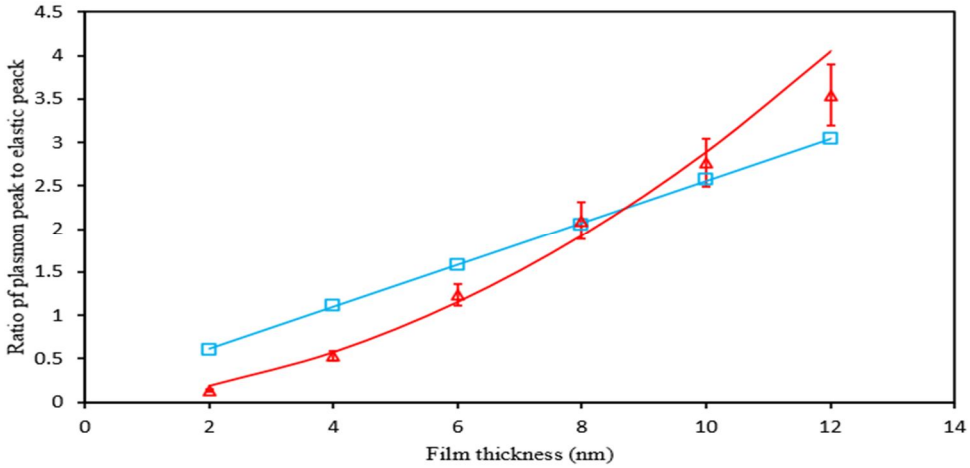

FIG. 8. Blue points = The ratio between the intensity of the first plasmon peak (integrated between 975 and 991 eV with a straight line under the peak to remove the background) and the zero-loss peak of Si (in transmission) for free-standing films with thicknesses from 2 to 12 nm at E_p = 1 keV. Red points represent the ratio between the second plasmon peak (integrated between 957 and 974 eV, also with the background removed) and the zero-loss peak of Si. The red lines are the fitted curves. The error bars for the blue points are the same size as those for the red points. A quadratic is fitted for the second plasmon peak (points between 2 and 10 nm) as this is what is expected from Eq. (1). The first plasmon peak was fitted with a straight line: intercept = 0.23 ± 0.42, slope = 0.22 ±.07 nm^{-1}. Fitting the second plasmon peak with $y = ax^2 + bx$: a = 0.024 ± 0.022 nm^{-2} and b = 0.05 ± 0.15 nm^{-1} Error bars are estimated according to an error in elastic and inelastic cross-sections of 10% in accordance with those used by Ref. [32].

Figures 9, 10, and 11 show the ratio between the intensity of the first plasmon peak (integrated after removing the background) and the zero-loss peak (elastic peak) for Si, Cu, and Au, respectively, at 1, 3, and 5 keV. One can see that the relationship between the two peaks is clearer. The ratio increases as the film thickness increases. It is also reduced as the primary energy increases.

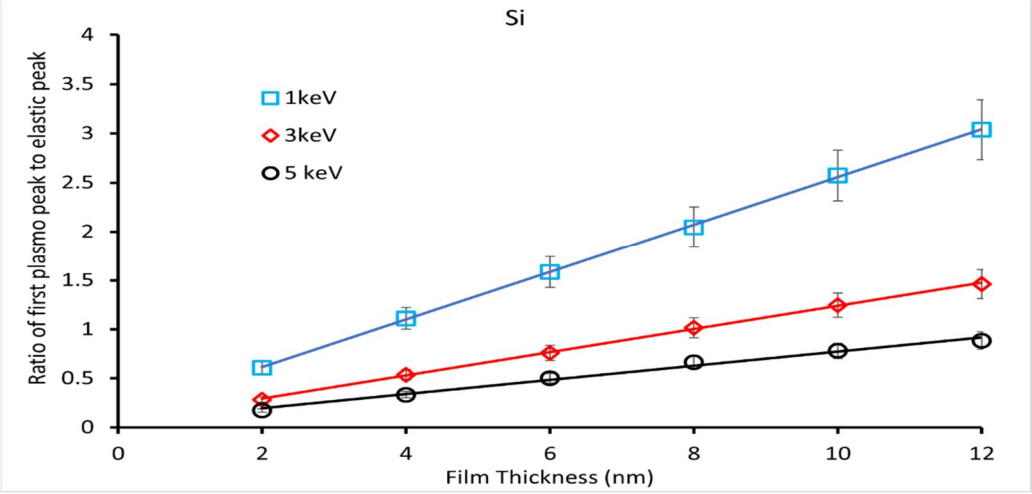

FIG. 9. The ratio between the intensity of the first plasmon peak and the zero-loss peak of Si (in transmission) for free-standing films with thicknesses from 2 to 12 nm at E_p = 1, 3, and 5 keV.

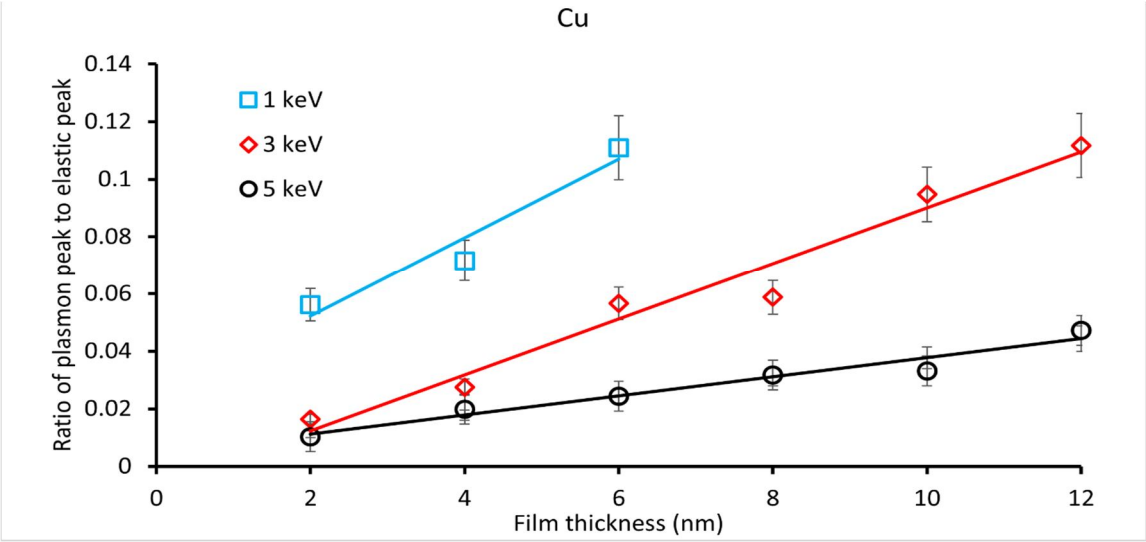

FIG. 10. The ratio between the intensity of the first plasmon peak and the zero-loss peak of Cu (in transmission) for free-standing films with thicknesses from 2 to 12 nm at E_p = 1, 3, and 5 keV.

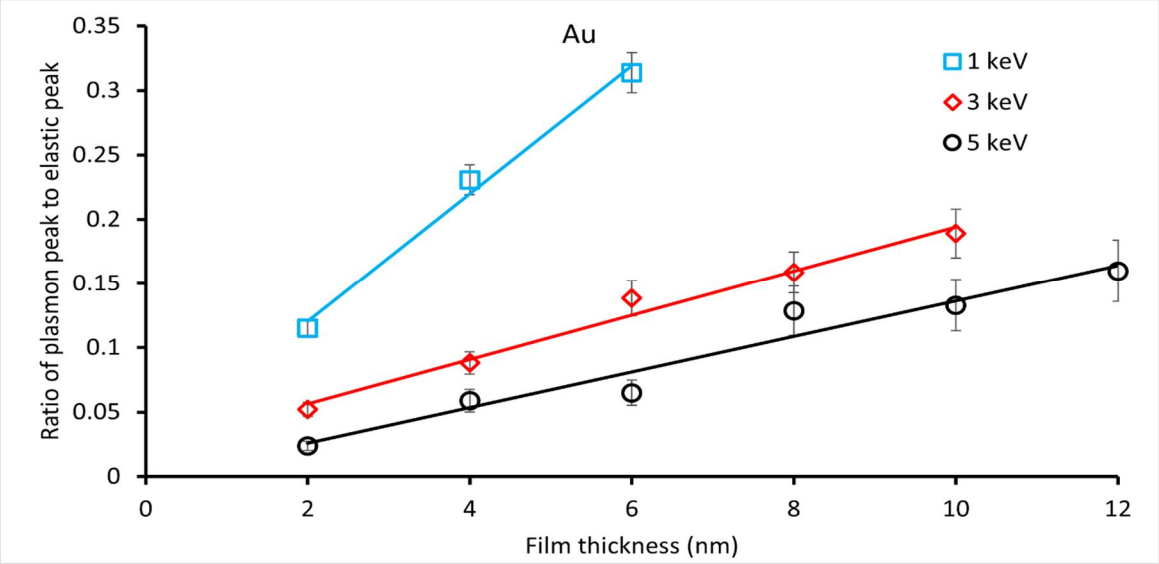

FIG. 11. The ratio between the intensity of the first plasmon peak and the zero-loss peak of Au (in transmission) for free-standing films with thicknesses from 2 to 12 nm at E_p = 1, 3, and 5 keV.

5. Conclusions

Transmitted electron spectra from free-standing thin films have been simulated from Si, Cu, and Au. The primary beam energies of 1, 3, and 5 keV were used. The current study suggests a direct method for determining the electron inelastic mean free path (IMFP) of materials at low primary electron energies. The proposed technique simplifies film thickness analysis by not requiring the IMFP values for the reference material. Free-standing films of Si, Cu, and Au were examined with thicknesses varying from 2 to 12 nm. The primary electron energies employed were 1, 3, and 5 keV.

The proposed method uses the log ratio of the area under the transmitted backscattered electron background to the area under the zero-loss peak (as used in TEM) to determine the inelastic mean free path (IMFP). Normally, electrons with energies of less than 50 eV are considered secondary electrons. The percentage error between the calculated results and the Monte Carlo given data was between 5% and 20%. It was also found that the ratio of the plasmon intensity to the zero-loss peak intensity followed a straight line when plotted against the film thickness. The observed straight-line behavior could also be used to determine film thicknesses and offers the advantage of quicker experimental signal acquisition. As with surface studies using Auger electron peaks, future consideration of the effects of elastic scattering, which introduces differences in the effective attenuation length (EAL) and inelastic mean free path (IMFP), may be required for primary beam energies less than 5 keV. Elastic scattering is stronger in materials with high atomic numbers, so we expect the influence of the EAL to be stronger in such materials. Further research is needed to establish a relationship between the slope of the straight line on one hand and the IMFP, the film atomic number, and thickness on the other.

The above approaches should allow better and faster estimates of film thickness using low primary energy TEM.

6. Acknowledgments

The authors would like to thank the ISG group (in particular Gurkan Myczko) for their help in setting up the Geant4 program at ETH Zürich. In addition, we thank Prof. M.M. El Gomati for useful discussions. Financial support by the FP7 People: Marie-Curie Actions Initial Training Network (ITN) SIMDALEE2 (Grant No. PITN 606988) is gratefully acknowledged.

References

[1] Boyes, E.D., Microsc. Microanal. 5 (1999) 674.

[2] Assa'd, A.M.D., Jordan J. Phys., 12 (1) (2019) 37.

[3] El Gomati, M.M. and El Bakush, T.A., Surf. Interface Anal., 24 (1996) 152.

[4] Assa'd, A.M.D. and Kawariq, H., Jordan J. Phys., 13 (2) (2020) 137.

[5] Geim, K. and Novoselov, K.S., Nat. Mater., 6 (2007) 183.

[6] Das, S., Robinson, J.A., Dubey, M., Terrones, H. and Terrones, M., Ann. Rev. Mater. Res., 45 (2015) 1.

[7] 2D Materials: Preparation, Characterization and Applications, Ed. I-Wen Peter Chen, Scientific Reports. (2019).

[8] Konvalina, I., Daniel, B., Zouhar, M., Paták, A., Piňos, J., Radlička, T., Frank, L., Müllerová, I. and Materna-Mikmeková, E., Microsc. Microanal., 26 (2020) 2636.

[9] Müllerová, I., Hovorka, M., Hanzlíková, R. and Frank, L., Mater. Trans., 51 (2010) 265.

[10] Kuhlman, W., Libera, M. and Gauthier, M., Microsc. Microanal., 6 (2000) 222.

[11] Sanche, L., J. Chem. Phys., 71 (1979) 4860.

[12] Naaman, R. and Sanche, L., Chem. Rev., 107 (2007) 1553.

[13] Walker, C.G.H., Konvalina, I., Mika, F., Frank, L. and Müllerová, I., Nucl. Instrum. Meth. B, 415 (2018) 17.

[14] Werner, W.S.M., Surf. Interface Anal., 35 (2003) 347.

[15] Cazaux, J., J. Appl. Phys., 111 (2012) 06490.

[16] Feenstra, R.M., Srivastava, N., Gao, Q., Widom, M., Diaconescu, B., Ohta, T., Kellogg, G.L., Robinson, J.T. and Vlassiouk, I.V., Phys. Rev. B, 87 (2013) 041406.

[17] Egerton, R.F., "EELS in the Electron Microscope". (Plenum Press, 1986).

[18] Botton, G.A., L'Esperance, G., Gallerneault, C.E. and Ball, M.D., J. Microsc., 180 (1995) 217.

[19] Egerton, R.F. and Malac, M., J. Electron Spectrosc., 143 (2005) 43.

[20] Tanuma, S., "Surface Analysis by Auger and X-ray Photoelectron Spectroscopy" Eds. D. Briggs and J. T. Grant (IM Publications and Surface Spectra Ltd; Chichester and Manchester, 2003), p. 259.

[21] Jablonski, A. and Powell, C.J., J. Electron Spectrosc., 281 (2017) 1.

[22] Tanuma, S., Shiratori, T., Kimura, T., Goto, K., Ichimura, S. and Powell, C.J., Surf. Interface Anal., 37 (11) (2005) 833–45.

[23] Tanuma, S., Yoshikawa, H., Okamoto, N. and Goto, K., J. Surf. Anal., 15 (2) (2008) 195–99.

[24] Shinotsuka, H., Tanuma, S., Powell, C.J. and Penn, D.R., Surf. Interface Anal., 47 (9) (2015) 871–88.

[25] https://delongamerica.com/.

[26] Kolosov, V.Y., Yushkova, A.A. and Bokuniaeva, A.O., AIP Conf. Proc., 2015, (2018) 020042.

[27] Kieft, E. and Bosch, E., J. Phys. D, 41 (2008) 215310.

[28] Agostinelli, S., Allison, J. , Amakoe, K. , Apostolakis, J. , Araujo, H., Arce, P., Asai, M., Axen, D., Banerjee, S., Barrand, G., Behner, F., Bellagamba, L., Boudreau, J., Broglia, L., Brunengo, A., Burkhardt, H., Chauvie, S., Chuma, J., Chytracek, R. and Cooperman, G., Nucl. Instrum. Meth. A, 506 (2003) 250.

[29] Mott, N.F. and Massey, H.S.W. “Theory of Atomic Collisions”. (Oxford University Press, London, 1965).

[30] Werner, W., Surf. Interface Anal., 31 (2001) 141.

[31] Palik, E.D., "Handbook of Optical Constants of Solids" (Academic, 1985).

[32] Walker, C.G.H., J. Matthew A.D. and El-Gomati, M.M., Scanning, 36 (2014) 241.